

Young Exosome Bio-Nanoparticles Restore Aging-Impaired Tendon Stem/Progenitor Cell Function and Reparative Capacity

Shanshan Jin, Yu Wang, Xiaolan Wu, Zixin Li, Lisha Zhu, Yuting Niu, Yongsheng Zhou,* and Yan Liu*

Aging impairs tendon stem/progenitor cell function and tendon homeostasis, however, effective treatments for aging-induced tendon diseases are lacking. Exosomes are naturally derived nanoparticles that contain bioactive molecules, and therefore, have attracted great interest in tissue engineering and regenerative medicine. In this study, it is shown that young exosomes secreted by stem cells from human exfoliated deciduous teeth (SHED-Exos) possess abundant anti-aging signals. These young bio-nanoparticles can alleviate the aging phenotypes of aged tendon stem/progenitor cells (AT-SCs) and maintain their tenogenic capacity. Mechanistically, SHED-Exos modulate histone methylation and inhibit nuclear factor- κ B to reverse AT-SC aging. In a naturally aging mouse model, systemic administration of SHED-Exo bio-nanoparticles retards tendon degeneration. Interestingly, local delivery of SHED-Exos-loaded microspheres confers anti-aging phenotypes, including reduced senescent cells and decreased ectopic bone formation, thereby functionally and structurally rescuing endogenous tendon regeneration and repair capacity in aged rats. Overall, SHED-Exos, as natural bioactive nanoparticles, have promising translational and therapeutic potential for aging-related diseases.

Tendon aging is frequently accompanied by extrinsic inflammation-aging harassment and intrinsic TSPC senescence, resulting in impaired reparative and regenerative capacities.^[2] Although the functional decline of senescent TSPCs is accepted well, an efficient and precise method to rejuvenate aged TSPC (AT-SC) function and recover aging-impaired tendon reparative capacity remains to be further explored.

Extracellular vesicles (EVs) are membrane-enclosed structures mainly that are classified into two main groups: exosomes and microvesicles. Among them, exosomes range from 40 to 150 nm in diameter and are mainly derived from the endosomal system,^[3] whereas microvesicles range from 100 to 1000 nm in diameter and are generated by shedding of the plasma membrane. EVs could facilitate intercellular communication by transferring mRNA, microRNA, proteins, and organelle cargoes into recipient

cells;^[4] therefore, EVs have been suggested as excellent candidates for therapeutic methods for tissue regeneration and repair. Recently, EVs have been proven to be beneficial components of young blood in extending the life span of mice, suggesting that some specific EVs may possess an anti-senescent function.^[5]

1. Introduction

Tendon aging is associated with the functional decline of cells and tissues, which causes tendon disorders, such as tendon rupture and limited mobility.^[1] Tendon homeostasis and repair rely on the function of tendon stem/progenitor cells (TSPCs).

S. Jin, Y. Wang, X. Wu, Z. Li, L. Zhu, Y. Liu
Laboratory of Biomimetic Nanomaterials
Department of Orthodontics
Peking University School and Hospital of Stomatology
National Center for Stomatology
National Clinical Research Center for Oral Diseases
National Engineering Research Center of Oral Biomaterials and Digital Medical Devices
Beijing Key Laboratory of Digital Stomatology
Research Center of Engineering and Technology for Computerized Dentistry Ministry of Health
NMPA Key Laboratory for Dental Materials
Beijing 100081, P. R. China
E-mail: orthoyan@bjmu.edu.cn

Y. Niu, Y. Zhou
Department of Prosthodontics
Peking University School and Hospital of Stomatology
National Center for Stomatology
National Clinical Research Center for Oral Diseases
National Engineering Research Center of Oral Biomaterials and Digital Medical Devices
Beijing Key Laboratory of Digital Stomatology
Research Center of Engineering and Technology for Computerized Dentistry Ministry of Health
NMPA Key Laboratory for Dental Materials
Beijing 100081, P. R. China
E-mail: kqzhoyush@hsc.pku.edu.cn

 The ORCID identification number(s) for the author(s) of this article can be found under <https://doi.org/10.1002/adma.202211602>.

DOI: 10.1002/adma.202211602

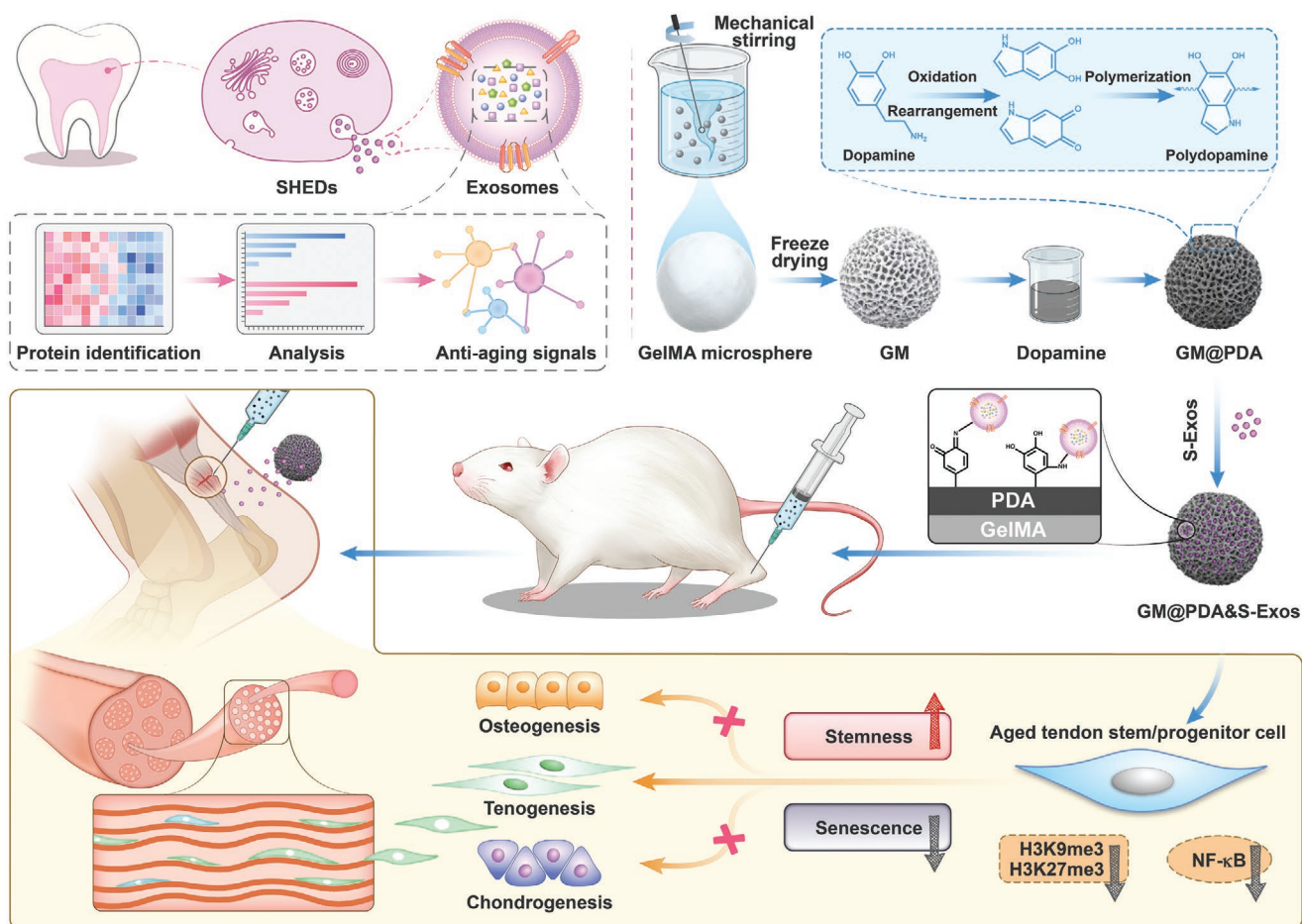
Stem cells from human exfoliated deciduous teeth (SHEDs) are relatively early-stage dental pulp mesenchymal cells. From the perspective of regenerative medicine, SHEDs present characteristics closest to those of cells during the embryonic period and maintain a primitive stemness status.^[6] Preliminary clinical studies have shown that SHEDs play a crucial role in the treatment of tissue injuries via paracrine function and possess significant advantages in clinical applications.^[7] In this study, we found that young exosomes derived from SHEDs (SHED-Exos) possessed abundant anti-aging signals. These bio-nanoparticles exhibited excellent anti-senescent effects and potently rescued senescent TSPCs into regenerative status at the physiological and epigenetic levels. Interestingly, SHED-Exos also promoted the tenogenic differentiation capacity of AT-SCs and inhibited their biased chondrogenic and osteogenic differentiation. Mechanistically, SHED-Exos decreased the accumulation of H3K9me3 and H3K27me3 to maintain the gene expression of stemness and tenogenic differentiation. In addition, SHED-Exo bio-nanoparticles also remarkably restrained the activation of nuclear factor (NF)- κ B to reduce inflammation-induced functional lesions. Systemic administration or local delivery of SHED-Exo bio-nanoparticles retarded tendon degeneration and promote tendon healing in aged mice and rats (Scheme 1).

2. Experimental Section

2.1. Isolation and Characterization of SHED-Exo Bio-Nanoparticles

Detailed methods are described in the Supporting Information.

Exosome nanoparticles were purified by several ultracentrifugation and filtration steps according to the previously published procedures.^[8] Briefly, SHEDs and human adult dental pulp stem cells (DPSCs) at passages 3–6 were utilized for the exosome isolation. The SHEDs and DPSCs were cultured in a complete medium with the fetal bovine serum for 48 h (with depletion of exosomes by 2 h centrifugation at 100 000g), culture supernatants of SHEDs and DPSCs were collected. Differential centrifugation was used to extract exosomes from culture supernatants of 2×10^7 SHEDs and DPSCs. The media of SHEDs and DPSCs were first centrifuged at 300g for 10 min to get rid of the cells and subsequently centrifuged at 3000g for 10 min to remove the apoptotic bodies and debris. After that, the supernatant was centrifuged at 10 000g for 30 min and filtered through a 0.22 μ m filter (Millipore, USA) to separate the microvesicles. The final supernatant was ultracentrifuged (Beckman Coulter, USA) at 120 000g for 70 min. The pellet was washed with



Scheme 1. a) Isolation procedure of SHED-Exo bio-nanoparticles and identification of their anti-aging signaling. b) Design and synthesis of the GM@PDA&SHED-Exo micro-nano composite that regenerates aged tendon injuries. c) Molecular mechanism of underlying stemness-promotion and anti-senescence of SHED-Exos on AT-SCs.

phosphate-buffered saline (PBS) to eliminate the contamination and centrifuged at 120 000g for another 70 min. The final pellet was resuspended in 200 μ L PBS and stored at -80°C .

The relative concentration of exosomes was detected by a BCA protein assay kit (BCA; Thermo Fisher Scientific, America). The morphology and size distribution of the extracted exosome nanoparticles was inspected by transmission electron microscopy (TEM; Leica JEM-1400, Japan) and the Nanosight system of ZetaView (Particle Metrix, German). Western blotting was performed to examine the specific exosome markers CD9, TSG101, and CD63, and cell lysates marker Calnexin.

2.2. Harvesting of SHED-Exo Proteins

2.2.1. Protein Extraction and Digestion

The SDT buffer (4%SDS, 100 mM Tris-HCl, 1 mM DTT, pH 7.6) was used for the sample lysis and protein extraction. The amount of protein was quantified with the BCA Protein assay kit (Bio-Rad, USA). The protein digestion by the trypsin was performed according to the filter-aided sample preparation procedure described by Matthias Mann. The digested peptides of each sample were desalted on C18 Cartridges (Empore SPE Cartridges C18, Sigma), concentrated by vacuum centrifugation, and reconstituted in 40 μ L of 0.1% (v/v) formic acid.

2.2.2. SDS-PAGE

20 μ g of protein for each sample were mixed with 5 \times loading buffer respectively and boiled for 5 min. The proteins were separated on 12.5% SDS-PAGE gel (constant current 14 mA, 90 min). The protein bands were visualized by Coomassie Blue R-250 staining.

2.2.3. LC-MS/MS Analysis

LC-MS/MS analysis was performed on a timsTOF Pro mass spectrometry coupled to Nanoelute (Bruker). The peptides were loaded onto a C18-reversed-phase analytical column (Thermo Scientific Easy Column) in 95% buffer A (0.1% formic acid in water) and separated with a linear gradient of buffer B (99.9% acetonitrile and 0.1% formic acid) at a flow rate of 300 mL min^{-1} . The mass spectrometer was operated in positive ion mode. The electrospray voltage applied was 1.5 kV. Precursors and fragments were analyzed at the TOF detector over a mass range of m/z 100–1700. The timsTOF Pro was operated in parallel accumulation serial fragmentation (PASEF) mode; PASEF mode data collection was performed based on the following parameters: ion mobility coefficient ($1/K_0$) value was set from 0.6 to 1.6 Vs cm^2 ; 1 MS and 10 MS/MS PASEF scans. The active exclusion was enabled with a release time of 24 s.

2.2.4. Identification and Quantitation of Proteins

The MS raw data for each sample were combined and searched using the MaxQuant 1.5.3.17 software for identification and

Table 1. MaxQuant identification and quantitation indexes.

Item	Value
Enzyme	Trypsin
Max missed cleavages	2
Fixed modifications	Carbamidomethyl (C)
Variable modifications	Oxidation (M)
Main search	6 ppm
First search	20 ppm
MS/MS tolerance	20 ppm
Database	Swissprot
Database pattern	Reverse
Include contaminants	True
protein FDR	≤ 0.01
Peptide FDR	≤ 0.01
Peptides used for protein quantification	Use a razor and unique peptides
Time window (match between runs)	2 min
protein quantification	LFQ
min. ratio count	1

Note: Intensity-based absolute quantification (iBAQ) and LFQ are two different methods for protein quantification provided by MaxQuant software. iBAQ Intensity reveals the level of protein expression in sample X based on the iBAQ algorithm, which is an approximation to the absolute protein concentration of the sample. LFQ Intensity reveals the level of protein expression in sample X based on the LFQ algorithm, which is often used in the comparison between groups.

quantitation analysis. Related parameters and instructions are as follows (Table 1):

2.3. Preparation and Characterization of GM and GM@PDA Microspheres

The gelatin methacryloyl (GelMA) microspheres (GM) were prepared by a modified emulsion-solvent extraction method.^[9] Briefly, 5% w/v GelMA solution was added dropwise into liquid paraffin containing Span 80 and stirred for 30 min to form a W/O emulsion at room temperature. The W/O emulsion was stirred continuously in an ice bath for another 30 min, thereby allowing the GM spheres to create a temporary physical cross-link. The GM spheres that were equipped with photoinitiator were exposed to 405 nm ultraviolet light to initiate photocrosslinking. After separating the oil phase with acetone, the GMs were processed by gradient-cooling and freeze-drying, and the porous microstructure was formed. To perform the surface modification, the GMs were immersed in dopamine solution (2 mg mL^{-1} in 10 mM Tris-HCl, pH 8.5) for 6 h, and the GM@PDA was obtained.

The gross appearance of microspheres was observed using a bright-field microscope (Nikon, Japan). A scanning electron microscope (JEOL JSM-7500F, Japan) was applied to examine the microstructure of the spheres, and the elemental mapping of oxygen (purple) and nitrogen (green) was performed at an exposure time of 180 s. The mean diameters of the microspheres were measured from multiple scanning electron microscopy (SEM) images using Image J software.

2.4. Exosome Adsorption and Release Assay

The exosome adsorption procedure was performed under aseptic conditions. To compare the ability of exosome adsorption between GM and GM@PDA, 5 mL SHED-Exos ($1000 \mu\text{g mL}^{-1}$) was added to 100 mg GM or GM@PDA and incubated at 4°C for 1–6 h. The adsorption kinetic of exosomes was examined at predetermined time points (1, 2, 3, 4, 5, and 6 h post-adsorption). At specific time points, 100 μL supernatant was collected and concentrated. To accumulate the release curve of GM and GM@PDA, 5 mg microsphere-exosome composites were soaked in 100 μL PBS and incubated at a horizontal shaker at $37 \pm 1^\circ\text{C}$, 60 rpm for 14 days. At predetermined time points (day 1, 3, 5, 7, 10, and 14), 80 μL supernatant was collected and the system was replenished with 80 μL fresh PBS; the concentration of exosomes in the supernatant was detected by BCA protein assay Kit.

2.5. Animal Models

Male three-month-old and eight-month-old Sprague–Dawley rats, 3-month-old C57BL/6J mice, and 6–8-week-old BLAB/c nude mice were bought from Wei Tong Li Hua Experimental Animal Center (China). And eight-month-old rats were further housed for ten months to be used for 18-month-old rat experiments. Male 18-month-old C57BL/6J mice were obtained from Biocytogen Pharmaceuticals. All the experimental procedures complied with animal welfare ethics and were approved by the Animal Use and Care Committee of Peking University (LA2020349). After surgery, all the animals were given food and water ad libitum.

2.5.1. Adhesion of GM@PDA&SHED-Exos on the Tendon Tissues

To verify the adhesion ability of the GM@PDA&SHED-Exos on the tendon tissues, the Achilles tendons and injected GM@PDA&SHED-Exos were harvested on the surface of the tendon tissues. After randomly shaking the SHED-Exos-loaded microspheres in all directions, pictures of the handled tissues were taken and recorded the process in video form (Movie S1, Supporting Information).

2.5.2. Retention of GM@PDA&SHED-Exos on Tendon Tissues In Vivo

The PKH26-labeled SHED-Exos alone or GM@PDA with PKH26-labeled SHED-Exos were injected into the Achilles tendons to evaluate the retention time. In short, the same amount (20 μL) of PKH26-SHED-Exos and GM@PDA&PKH26-SHED-Exos were injected into the rat Achilles tendons, and the IVIS spectroscopy system was used to detect the fluorescence. The excitation wavelength was 551 nm, and the emission wavelength was 567 nm. The images were obtained on days 1, 3, 7, and 14. The rat Achilles tendons were harvested six hours after injection, and the IVIS imaging was carried out alone to confirm that GM@PDA could adhere to the tendon tissues.

2.5.3. In Situ Tendon Repair with GM@PDA&SHED-Exos in Collagenase-I-Induced Tendinopathies in Three-Month-Old Young Adult Mice

Three-month-old mice were injected with collagenase I solution to induce tendinopathies. GM@PDA&SHED-Exos suspended in 20 μL PBS were injected into the injured tendons. As the control, the contralateral tendons of recipient mice were similarly injured and injected with GM@PDA. More than four mice per group were chosen for each time point.

2.5.4. In Situ Tendon Regeneration with GM@PDA&SHED-Exos in Aged Rats

A partial cut was made in the Achilles tendons in 18-month-old rats. GM@PDA&SHED-Exos suspended in 50 μL PBS was injected into the injured tendons. Each group had four rats for each time point.

To visualize the distribution and retention of microspheres in the injured tendons after injection, the PKH26 was used to label SHED-Exos in the synthesis process of GM@PDA&SHED-Exos, and GM@PDA&PKH26-SHED-Exos were obtained. The rats were injected with GM@PDA&PKH26-SHED-Exos, and the in vivo microsphere distribution was analyzed with a fluorescence imaging system at the indicated time.

2.5.5. Macroscopic Evaluation of Regenerated Tendons

In the eighth week postoperatively, the rats were euthanized, and the Achilles tendons were exposed fully. Then, the full-length tendon complexes, including partial gastrocnemius and calcaneus, were harvested and photographed using a camera (Nikon, Japan).

2.6. Histology and Immunofluorescence

The tissue specimens were fixed in 4% paraformaldehyde, washed with running water, dehydrated in a graded ethanol series, vitrified with dimethyl benzene, and embedded in the paraffin. The paraffin sections (6 μm) were deparaffinized in xylene, hydrated with gradient ethanol, and stained with standard hematoxylin and eosin (HE), Alcian blue, or Masson staining procedures.

The harvested Achilles tendons were fixed immediately in 10% neutral buffered formalin for 24 h, dehydrated using the gradient alcohol, and embedded in the paraffin blocks for immunostaining tissues. Histological sections with the 8 μm thickness were gathered using a microtome. Enzyme-activated antigen retrieval was performed by placing the paraformaldehyde-fixed samples in a 37°C water bath for 45 min and cooling the slides at room temperature for 10 min. Then, the sections were blocked in TBST with 5% NDS and 0.1% triton for 1 h and incubated overnight with primary antibodies. Primary antibodies used in this study were listed in Table S1 (Supporting Information). Non-immune immunoglobulins of the same isotype as the primary antibodies were used as a negative control.

Next, appropriate Alexa Fluor 488- and Alexa Fluor 594-conjugated secondary antibodies (Thermo Fisher Scientific, 1:400) were utilized for 1.5 h at room temperature. After that, nuclei were stained with DAPI (ZSGB-BIO) for 10 min in the dark. The confocal microscopy images were acquired with a Zeiss laser-scanning microscope 710 or a Leica TCS SP8 STED confocal microscope.

2.7. Microcomputed Tomography (Micro-CT)

The hindlimbs from the rats and mice were fixed in 4% paraformaldehyde and analyzed by micro-CT (Skyscan 1172). The scanner was set at a voltage of 80 kV and a resolution of 18 μm per pixel. The images were analyzed by NRecon, CTAn, and CTVol software.

2.8. Scanning Electron Microscopy

The microstructure of neo-tissues was examined by SEM (Hitachi SU8020, Japan) at 10 kV. Briefly, the tissues were prefixed in 2.5% glutaraldehyde in PBS (pH 7.4) at 4 $^{\circ}\text{C}$ for 12 h and washed thrice with PBS. All the samples were dehydrated in a graded series of ethanol (50–100%), critical-point dried, and sputter-coated with gold for 2 min at 20 mA.

2.9. Strength by Grip Test

The rats were allowed to grasp a horizontal grid connected to a dynamometer (Sansbio, CAT#SA417) with two hindlimbs and were pulled backward five times. The force applied to the grid each time before the animal lost its grip was recorded in Newton.

2.10. Achilles Functional Index

To evaluate the healing outcomes of the Achilles tendons, their motility was assessed by Achilles functional index (AFI) at one, four, and eight weeks postoperatively, adopting a method from a previous study.^[10] Briefly, a restrictive roadway (100 cm long and 25 cm wide) was covered with white paper. After their hind paws were evenly dipped with the black ink, the rats could walk freely, printing black footprints on the white paper. To quantify the AFI of rats or mice, footprints were scanned (Epson Scanner, Japan). Footprint parameters including print length (PL), toe spreading length (defined as the distance between the first and fifth toes, TS), and intermediary toe spreading length (defined as the distance between the second and fourth toes, IT) were acquired and defined. Then, according to the difference between the normal (N) and the experimental values (E), three footprint dimension factors (PLF, TSF, ITF) could be obtained according to the following equations:

$$\text{PLF} = \frac{(\text{NPL} - \text{EPL})}{\text{EPL}} \quad (1)$$

$$\text{TSF} = \frac{(\text{ETS} - \text{NTS})}{\text{NTS}} \quad (2)$$

$$\text{ITF} = \frac{(\text{EIT} - \text{NIT})}{\text{NIT}} \quad (3)$$

finally, the AFI was calculated according to an established equation

$$\text{AFI} = 74 (\text{PLF}) + 161 (\text{TSF}) + 48 (\text{ITF}) \quad (4)$$

2.11. Statistical Analysis

Statistical analysis was performed using GraphPad Prism software 8 (GraphPad Software, Inc.). All the experimental results were expressed as the mean \pm standard deviation (SD). Differences between groups were assessed by the two-sided Student's *t*-test (for two-group comparisons) or the one-way analysis of variance (ANOVA) with Tukey's test (for more than two-group comparisons). Statistical significance was set at $p < 0.05$.

3. Results

3.1. Young SHED-Exo Bio-Nanoparticles Rejuvenate AT-SCs and Improve Their Tenogenic Differentiation Capacity

To obtain young exosome bio-nanoparticles, SHEDs, similar to embryonic cells, were expanded in an EV-depleted medium. Ultracentrifugation and filtration steps were conducted to extract exosomes from culture supernatants. Adult exosomes derived from human adult dental pulp stem cells (DPSC-Exos) were used as the controls. TEM demonstrated that both SHED-Exo and DPSC-Exo nanoparticles exhibited typical exosome morphologies with round bulging structures. Nanoparticle tracking analysis revealed cellular particles of nano-size of ≈ 125 nm and the absence of significant differences between the groups (Figure 1a). Both SHED-Exos and DPSC-Exos were positive for TSG101, CD63, and CD9 (Figure 1b). Because the preliminary screening experiments showed that SHED-Exos possessed better pro-proliferation and anti-aging functions than DPSC-Exos in vitro (Figure S1a–d, Supporting Information), we performed proteomics analysis of DPSC-Exos and SHED-Exos (Table 1), respectively. SHED-Exos contained a significantly greater number of differentially expressed proteins ($p < 0.05$) than DPSC-Exos (Figure 1c). Gene ontology enrichment analysis revealed that the SHED-Exos accumulated proteins for genes associated with cell proliferation, metabolic process, response to stimulus, developmental process, and antioxidant activity (Figure S2a, Supporting Information). Furthermore, a Kyoto Encyclopedia of Genes and Genomes (KEGG) analysis revealed that longevity regulating pathway, mitophagy, nicotinate, and nicotinamide metabolism-related pathway were enriched in SHED-Exos. In contrast, several potential pathways that are associated with senescence development, including the transforming growth factor- β signaling pathway, the Janus kinase-signal transducer and activator of the transcription signaling pathway, and Th17 cell differentiation evidently were increased

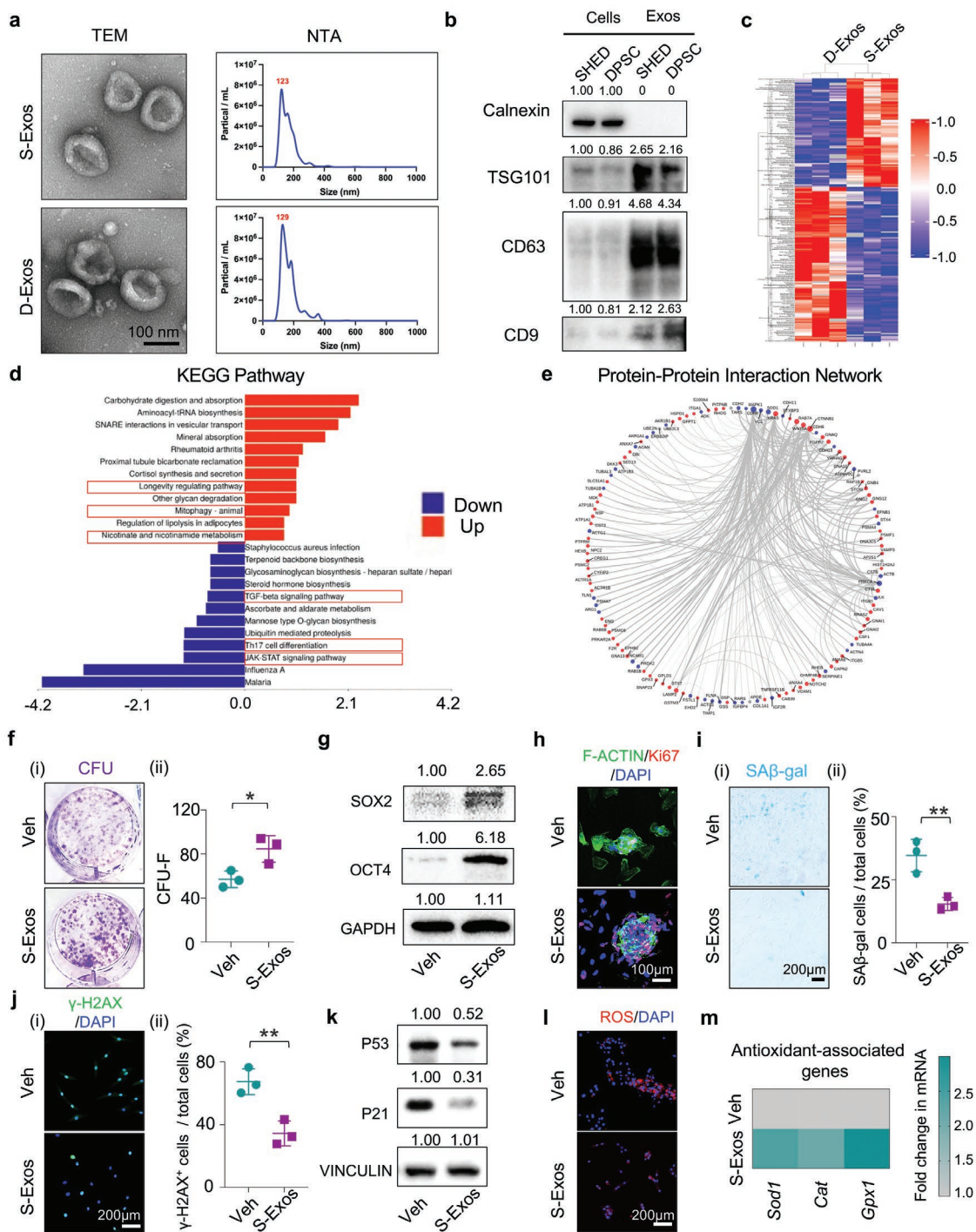


Figure 1. SHED-Exo bio-nanoparticles promote AT-SC stemness and delay AT-SC senescence. a) TEM images and nanoparticle tracking analysis (NTA) of SHED-Exos (S-Exos) and DPSC-Exos (D-Exos) nanoparticles ($n = 3$ biologically independent samples). b) Western blotting of the expression of calnexin and surface protein markers including CD63, TSG101, and CD9 ($n = 3$ biologically independent samples). c) Significantly upregulated and downregulated proteins (SHED-Exos vs. DPSC-Exos). d) KEGG analysis of upregulated and downregulated proteins in SHED-Exos compared to those in DPSC-Exos. e) PPI network based on differential-expressed proteins associated with the significant pathways using the STRING database. f) i) Colony-forming unit-fibroblasts (CFU-Fs) of vehicle- (Veh) and SHED-Exos-treated AT-SCs. ii) Semi-quantification of (i) ($n = 3$ biologically independent samples). g) Western blotting of SOX2 and OCT4 in vehicle- and SHED-Exos-treated AT-SCs ($n = 3$ biologically independent samples). h) Immunofluorescence staining of Ki67 and F-actin of vehicle- and SHED-Exos-treated AT-SC spheroids. i) i) SA β -gal staining and ii) Semi-quantification of vehicle- and SHED-Exos-treated AT-SCs. Blue cells are senescent cells. ($n = 3$ biologically independent samples). j) i) Immunofluorescence staining of γ -H2AX of vehicle- and SHED-Exos-treated AT-SCs. ii) Semi-quantification of (i) ($n = 3$ biologically independent samples). k) Western blotting of P53 and P21 in vehicle- and SHED-Exos-treated AT-SCs ($n = 3$ biologically independent samples). l) Immunofluorescence staining of ROS of vehicle- and SHED-Exos-treated AT-SCs. m) RT-qPCR of antioxidant-related gene expression *Sod1*, *Cat*, and *Gpx1* ($n = 3$ independent experiments). Data are represented as mean \pm SD. Statistical significance was determined by a two-sided Student's *t*-test (* $p < 0.05$; ** $p < 0.01$; *** $p < 0.001$).

in DPSC-Exos (Figure 1d). To further explore the relationship between the differential proteins and the anti-aging effect, we selected differentially-expressed proteins associated with autophagy, longevity regulating pathway, signaling pathways regulating the pluripotency of stem cells, the wingless-related integration site signaling pathway and the adenosine monophosphate-activated protein kinase signaling pathway, which have been demonstrated to be involved in counteracting the aging process and promoting cell proliferation. Subsequently, we generated a protein-protein interaction network (PPI) based on the STRING database. The PPI analysis revealed that these differentially expressed proteins maintained a positive and interactive relationship (Figure 1e). Overall, our results suggested that compared to DPSC-Exos, SHED-Exos possesses a great number of anti-aging signals that possibly better rescue senescent cells.

Next, we investigated whether young SHED-Exo bio-nanoparticles could rescue the phenotypic characteristics of AT-SCs. First, to demonstrate that these nanoparticles could be absorbed by AT-SCs, SHED-Exos were labeled with a membrane-binding fluorescent dye PKH26 and subsequently added to the culture medium with AT-SCs. Immunofluorescence staining showed that SHED-Exo nanoparticles were taken up by the AT-SCs, showing strong colocalization of PKH26 and SHED-Exos in the AT-SCs (Figure S2b, Supporting Information). These AT-SCs were subsequently treated with SHED-Exos every second day for seven days. Compared to the untreated group, the SHED-Exo-treated AT-SCs showed markedly elevated self-renewal and proliferation capacities, as evidenced by larger amounts of colonies and marked increase in the number of Ki67⁺ cells (Figure 1f, Figure S2c, Supporting Information). Reverse transcription-quantitative polymerase chain reaction (RT-qPCR) demonstrated that the SHED-Exo treatment significantly enhanced the expression of *Sox2* and *Oct4* in the AT-SCs, which was consistent with western blotting results, suggesting that SHED-Exo nanoparticles enhanced AT-SC stemness (Figure 1g, Figure S2d, Supporting Information). Interestingly, the SHED-Exo treatment promoted larger amounts of spheroid formation with increased radius and higher expression of Ki67 (Figure 1h). Moreover, the SHED-Exo treatment ameliorated multiple hallmarks of aging, as evidenced by the following findings: i) markedly reduced SA β -gal-positive cells (Figure 1i); ii) repressed DNA damage responses, as indicated by the reduction of the number of γ H2AX⁺ cells (Figure 1j); iii) significantly decreased the protein expression of aging-associated factors P53 and P21 (Figure 1k); iv) reduced the expression of *Il6*, *Il1 β* , and *Ccl2* indicated declined senescence-associated secretory phenotype, which has been demonstrated to disrupt the tissue microenvironment and compromise tissue structure (Figure S2e, Supporting Information).^[11] Excessive accumulation of reactive oxygen species (ROS) in TSPCs has been reported to affect TSPC renewal ability, resulting in the loss of stemness.^[12] Our results showed that treatment with SHED-Exo nanoparticles decreased the accumulation of ROS in the AT-SCs (Figure 1l). Moreover, SHED-Exo treatment also enhanced the mRNA expression of antioxidant-associated genes including superoxide dismutase 1 (*Sod1*), catalase (*Cat*), and glutathione peroxidase (*Gpx1*), which have been shown to influence stem cell senescence and induce tendinopathy progression (Figure 1m).^[13]

TSPC senescence is frequently accompanied by a biased differentiation direction, as reflected by the declination of tenogenic differentiation, and enhancement of chondrogenic and osteogenic differentiation.^[1] In this study, SHED-Exo bio-nanoparticles reversed the declined tenogenic differentiation of the AT-SCs, as evidenced by the enhanced collagen deposition and the increased expression of tenogenesis-related markers collagen type I (COL1) and fibromodulin (FMOD) (Figure 2a,b). To further explore the differentiation capacity of SHED-Exo-treated AT-SCs ex vivo, we subcutaneously transplanted aged AT-SCs in nude mice. HE and immunofluorescence stainings showed that SHED-Exo-treated AT-SCs displayed a great number of new tendon collagen fibers and higher expression of tenogenesis-related markers scleraxis (SCX) and tenomodulin (TNMD) (Figure 2c,d). Noticeably, SHED-Exo nanoparticles also inhibited the biased differentiation of the AT-SCs. Compared to the untreated AT-SCs (vehicles), the SHED-Exo-treated AT-SCs showed decreased osteogenic differentiation capacity, as revealed by the reduced calcium nodule formation, and decreased expression of the osteogenesis-related factors including run-related transcription factor 2 (*Runx2*) and bone gla protein (*Bglap*) at the mRNA levels, which was consistent with western blotting results (Figure 2e–g). Moreover, the AT-SCs from the SHED-Exo-treated group exhibited poorer chondrogenic capacity in a chondrogenic induction culture, as evidenced by the weaker Alcian blue staining and the decreased expression of chondrogenic markers sry-box transcription factor 9 (SOX9) and collagen type II (COL2) (Figure 2h,i). These findings confirmed that SHED-Exos could reverse biased osteogenic and chondrogenic differentiation of AT-SCs.

3.2. SHED-Exos Reverse AT-SC Aging by Decreasing H3K9me3 and H3K27me3 Abundance and Suppressing NF- κ B

Given the role of histone modification in the aging process,^[14] we investigated whether SHED-Exo bio-nanoparticles exerted their anti-senescent function by modifying histone markers. Immunofluorescence staining showed that the SHED-Exo treatment significantly reduced the H3K9me3 and H3K27me3 levels in the AT-SCs isolated from 18-month-aged rats (Figure 3a,b). Downregulation of H3K9me3 and H3K27me3 was confirmed by western blotting analysis (Figure 3c). To examine whether the anti-senescent effect was dependent on the modulation of histone methylation, we treated the isolated AT-SCs with a pan-inhibitor of Jumonji histone demethylases, JIB 04. The application of 2 μ m JIB 04 for four days counteracted the downregulation effect of SHED-Exos on the H3K9me3 and H3K27me3 at the protein level (Figure 3d). The western blotting results showed that treatment with JIB 04 counteracted the upregulation of the SOX2 and OCT4 protein levels (Figure 3e). Moreover, the number of CFU-Fs declined significantly (Figure 3f). Interestingly, the inhibitory effect on P21 by SHED-Exos was also counteracted by the supplementation with JIB 04 (Figure 3g). We subsequently examined AT-SC differentiation after stimulation with JIB 04. Immunofluorescence staining showed that the increased expression of tenogenesis-related markers COL1 and FMOD declined after the supplementation with JIB 04 (Figure 3h). In contrast, after JIB 04 intervention,

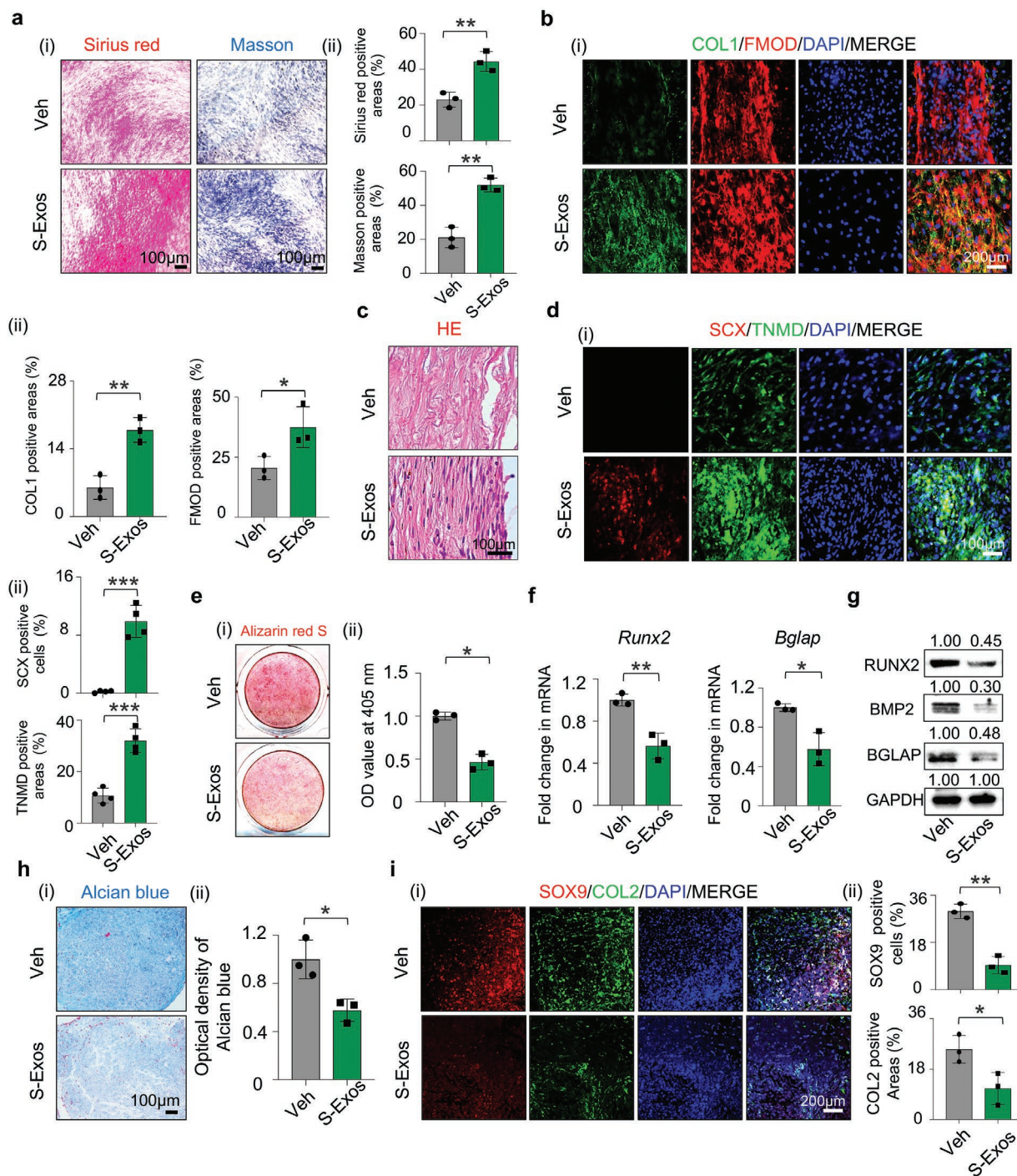


Figure 2. SHED-Exo bio-nanoparticles maintain AT-SC tenogenic capacity and inhibit its chondrogenic and osteogenic differentiation. a) i) Sirius red and Masson's trichrome stainings of vehicle- and SHED-Exo-treated AT-SCs after 14-day tenogenic induction. ii) Semi-quantification of (i) ($n = 3$ biologically independent samples). b) i) Immunofluorescence staining of COL1 and FMOD of vehicle- and SHED-Exo-treated AT-SCs after 14-day tenogenic induction. ii) Semi-quantification of (i) ($n = 3$ biologically independent samples). c) HE staining of parallel-aligned collagen structure formed by subcutaneous transplantation of vehicle- and SHED-Exo-treated AT-SCs. d) i) Immunofluorescence staining of SCX and TNMD in vehicle- and SHED-Exo-treated AT-SC groups. ii) Semi-quantification of (i) ($n = 4$ mice per group). e) i) Alizarin red staining of vehicle- and SHED-Exo-treated AT-SCs after 14-day osteogenic induction. ii) Semi-quantification of (i) ($n = 3$ biologically independent samples). f) RT-qPCR of osteogenesis-related gene expression of *Runx2* and *Bglap* in vehicle- and SHED-Exo-treated AT-SCs after 14-day osteogenic induction. ($n = 3$ independent experiments). g) Western blotting of osteogenesis-related gene expression of RUNX2, BGLAP, and BMP2 in vehicle- and SHED-Exo-treated AT-SCs after 14-day osteogenic induction. ($n = 3$ independent experiments). h) i) Alcian blue staining of Vehicle- and SHED-Exo-treated AT-SCs after 14-day chondrogenic induction. ii) Semi-quantification of (i) ($n = 3$ biologically independent samples). i) i) Immunofluorescence staining of SOX9 and COL2 of vehicle- and SHED-Exo-treated AT-SCs after 14-day chondrogenic induction. ii) Semi-quantification of (i) ($n = 3$ biologically independent samples). Data are represented as mean \pm SD. Statistical significance was determined by a two-sided Student's *t*-test (* $p < 0.05$; ** $p < 0.01$; *** $p < 0.001$).

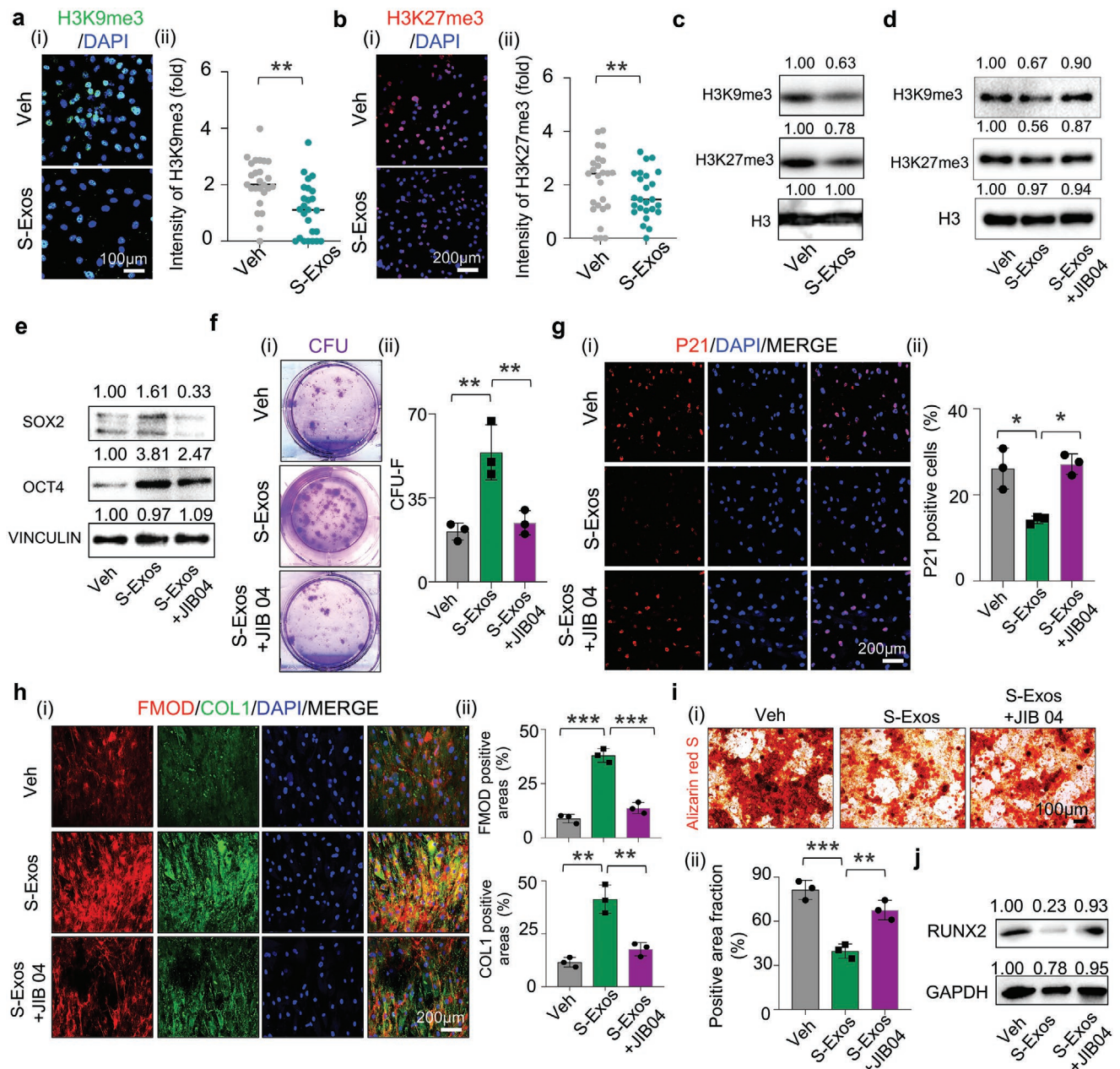


Figure 3. SHED-Exo bio-nanoparticles delay AT-SC senescence and maintain AT-SC tenogenic capacity by decreasing H3K9me3 and H3K27me3 abundance. a) i) Immunofluorescence staining of H3K9me3 of vehicle- and SHED-Exos-treated AT-SCs. ii) Semi-quantification of (i) ($n = 3$ biologically independent samples). b) i) Immunofluorescence staining of H3K27me3 of vehicle- and SHED-Exos-treated AT-SCs. ii) Semi-quantification of (i) ($n = 3$ biologically independent samples). c) Western blotting of H3K9me3 and H3K27me3 in vehicle- and SHED-Exos-treated AT-SCs. ($n = 3$ independent experiments). d) Western blotting of H3K9me3 and H3K27me3 in vehicle-, SHED-Exos-treated-, and SHED-Exos + JIB 04-treated AT-SCs. ($n = 3$ independent experiments). e) Western blotting of SOX2 and OCT4 in vehicle-, SHED-Exos-treated-, and SHED-Exos + JIB 04-treated AT-SCs. ($n = 3$ independent experiments). f) i) CFU-F assay of vehicle-, SHED-Exos-treated-, and SHED-Exos + JIB 04-treated AT-SCs. ii) Semi-quantification of (i) ($n = 3$ biologically independent samples). g) i) Immunofluorescence staining of P21 in vehicle-, SHED-Exos-treated-, and SHED-Exos + JIB 04-treated AT-SCs. ii) Semi-quantification of (i) ($n = 3$ biologically independent samples). h) i) Immunofluorescence staining of COL1 and FMOD of vehicle-, SHED-Exos-treated-, and SHED-Exos + JIB 04-treated AT-SCs after 14-day tenogenic induction. ii) Semi-quantification of (i) ($n = 3$ biologically independent samples). i) i) Alizarin red staining of vehicle-, SHED-Exos-treated-, and SHED-Exos + JIB 04-treated AT-SCs after 14-day osteogenic induction. ii) Semi-quantification of (i) ($n = 3$ biologically independent samples). j) Western blotting of protein levels of RUNX2 of vehicle-, SHED-Exos-treated-, and SHED-Exos + JIB 04-treated AT-SCs after 14-day osteogenic induction. ($n = 3$ independent experiments). Data are represented as mean \pm SD. Statistical significance was determined by two-sided Student's t -test (a,b), or one-way ANOVA with Tukey's test (f–j). (* $p < 0.05$; ** $p < 0.01$; *** $p < 0.001$).

osteogenic differentiation of the AT-SCs was remarkably elevated, as evidenced by the stronger Alizarin red staining and the higher protein levels of RUNX2 (Figure 3i,j).

NF- κ B is regarded as a core regulator of inflammatory diseases and aging-induced tissue degeneration.^[15] Recently, studies have observed that NF- κ B was activated in senescent TSPCs, which could contribute to the hypofunction of AT-SCs.^[16] Therefore, we explored whether SHED-Exo bio-nanoparticles could curb the activation of the NF- κ B signaling pathway. Treatment with SHED-Exos in vitro inhibited the phosphorylation of p65 and nuclear translocation of p65 in AT-SCs (Figure S3a,b, Supporting Information). NF- κ B is frequently activated by proinflammatory cytokines such as tumor necrosis factor (TNF) and interleukin (IL)-17 in chronic inflammatory diseases or tissue injuries.^[17] To determine whether SHED-Exos could inhibit the TNF-activated I κ B kinase–NF- κ B signaling pathway in AT-SCs, we applied the TNF to AT-SCs with or without the SHED-Exo pretreatment. As shown in Figure S3c (Supporting Information), SHED-Exo nanoparticles inhibited the TNF-induced p65 phosphorylation in the AT-SCs. Immunofluorescence staining confirmed that SHED-Exos inhibited p65 activation, compared to the vehicle control (Figure S3d, Supporting Information). RT-qPCR revealed that SHED-Exos significantly reduced the expression of inflammatory genes *Il-6* and *Ccl5* (Figure S3e, Supporting Information). Subsequently, we examined whether SHED-Exos could restore the impaired function of AT-SCs under inflammation stimulation. Colony-forming experiments showed that SHED-Exo treatment rescued TNF-induced impairment of AT-SC self-renewal, as evidenced by the greater number of colony units (Figure S3f, Supporting Information). Persistent TNF stimulation resulted in early maturing senescence of the AT-SCs, which was partially weakened by the SHED-Exo treatment, as reflected by a reduced ratio of SA- β -gal-stained cells and decreased protein levels of P53 and P21 (Figure S3g,h, Supporting Information). Moreover, Sirius red staining revealed that the SHED-Exo treatment could efficiently remedy the weakened tenogenic differentiation capacity that was induced by inflammatory stimuli (Figure S3i, Supporting Information).

3.3. Bioactive SHED-Exo Nanoparticles Retard Degenerative Tendinopathies in Aged Mice

Spontaneous calcification of tendons occurs with aging, which may result from the biased differentiation of AT-SCs and chronic, lower inflammation stimulus.^[2] To examine whether SHED-Exo bio-nanoparticles could ameliorate the progression of aged tendon degeneration, we intravenously injected these bio-nanoparticles in aged mice for eight weeks (Figure S4a, Supporting Information). Compared with the untreated mice, hindlimb function in the SHED-Exos-treated mice was improved, as evidenced by the increased level of grip strength (Figure S4b, Supporting Information). Micro-CT analysis revealed an apparent reduction in heterotopic ossification in the SHED-Exos-treated tendons (Figure S4c, Supporting Information). HE staining revealed a significant improvement in the collagen arrangement in the SHED-Exos-treated group, which was accompanied by higher protein levels of tenogenesis-related

markers TNMD and tenascin-C (TNC) (Figure S4d,e, Supporting Information). Alcian blue staining and immunofluorescence staining of AGGRECAN revealed that marked reduction in proteoglycan accumulation and cartilage matrix formation in the SHED-Exos-treated group (Figure S4f,g, Supporting Information). Subsequently, the senescent and inflammatory status of the tendons was further explored. Immunofluorescence showed that the tendons from the SHED-Exos-treated group exhibited markedly lower expression levels of the senescence-related marker P21 after two-month administration of SHED-Exos compared to the vehicle control (Figure S4h, Supporting Information). RT-qPCR results revealed that administration of SHED-Exos remarkably reduced the gene expression of inflammatory cytokines *Tnf- α* and *Il-6* in tendon tissues (Figure S4i, Supporting Information). Moreover, immunofluorescence staining showed that the SHED-Exo administration remarkably reduced the percentages of H3K9me3, H3K27me3, and p65 positive cells in the Achilles tendon sections from 18-month-old aged mice (Figure S4j,k, Supporting Information). Overall, the systemic administration of bioactive SHED-Exo nanoparticles partially rescued the aging-induced tendon degeneration in aged mice.

3.4. Hydrogel Microspheres Loaded with SHED-Exo Nanoparticles Efficiently Rejuvenate AT-SCs and Maintain Their Tenogenic Differentiation

To explore the anti-senescent and pro-reparative effects of the local administration of SHED-Exos, GelMA hydrogel microspheres were fabricated to load the bio-nanoparticles, owing to their excellent biocompatibility, low immunogenicity, low cytotoxicity, and easy procurement.^[18] To optimize the local in situ release of effective drugs from these microspheres,^[19] GelMA was surface-modified by polydopamine (PDA) polymerization because of its excellent adhesive properties (Figure 4a,b).^[20] As shown in Figure 4c, GelMA microspheres (GM) displayed a white appearance, whereas the microspheres modified by PDA (GM@PDA) were light brown. The obtained monodisperse microspheres possessed spherical shapes with sizes of $136.4 \pm 12.8 \mu\text{m}$, and an average diameter of GM@PDA was $141.0 \pm 15.5 \mu\text{m}$. SEM showed that both GM and GM@PDA exhibited porous structures. Elemental mapping showed that nitrogen signals (in green) on the surface of GM@PDA indicated PDA coating (Figure 4d,e). Accordingly, the uniform PDA did not damage the porous structure of the microspheres, which could provide a necessary condition for exosome loading. Fluorescence staining confirmed that green-stained TSPCs and red-stained SHED-Exos were efficiently loaded onto GM@PDA (Figure 4f). To assess the potential of therapeutic applications of the injectable microspheres, we investigated the in vitro cytotoxicity of GM@PDA on TSPCs. Living/dead experiments and cell counting kit-8 (CCK-8) tests were conducted to assess the biocompatibility of the composite microspheres. As shown in Figure 4g, the cell density in the GM@PDA and GM@PDA&SHED-Exos groups increased, and few dead cells were observed during the three-day cell culture. The CCK8 quantitative experiments demonstrated that GM@PDA&SHED-Exos remarkably enhanced the cell proliferation activity on days

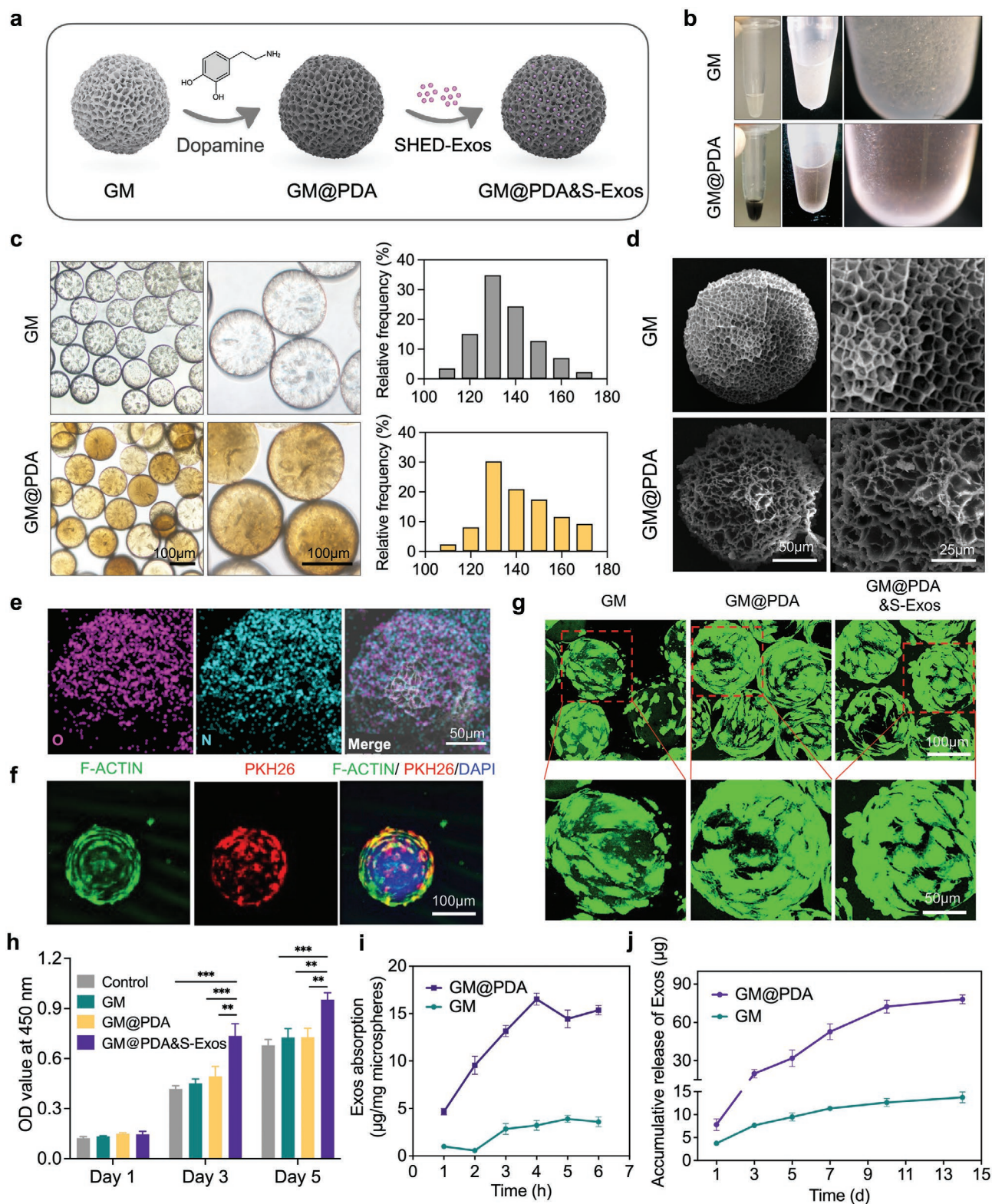


Figure 4. Characterization of GM@PDA&SHED-Exo micro-nano composites. a) Scheme of synthesis of GM@PDA&SHED-Exos. b) Overall views of dispersed GM and GM@PDA solutions. The left column is the gross morphology and the right two columns show the optical images. c) Overall views and particle size distributions of dispersed GM and GM@PDA. d) SEM images of dispersed GM and GM@PDA. e) Elemental mapping images of GM@PDA&SHED-Exos. f) Immunofluorescence images of TSPCs (green) cultured on GM@PDA&SHED-Exos (red). g) Live/dead assay staining of TSPCs cultured on various microspheres. h) Cell proliferation study on TSPCs cultured on various microspheres using CCK-8. i) Loading efficiency curves over time for GM and GM@PDA. j) Release profiles of SHED-Exos from GM and GM@PDA. Data are represented as mean ± SD. Statistical significance was determined by two-sided Student's *t*-test (i,j), or one-way ANOVA with Tukey's test (h) (* $p < 0.05$; ** $p < 0.01$; *** $p < 0.001$).

3 and 5 (Figure 4h). These results further suggest that the composite microspheres possess outstanding biocompatibility. We systematically studied the loading efficiency and release profile of exosomes from the GM and GM@PDA. The porous structure and PDA modification made the GM@PDA microspheres reach the maximum loading rate of $16.52 \pm 0.63 \mu\text{g mg}^{-1}$ microsphere after soaking for 4 h. In comparison, the GM reached its maximum loading rate of $3.59 \pm 0.51 \mu\text{g mg}^{-1}$ microspheres only after soaking for 6 h (Figure 4i). The in vitro release of exosomes was carried out at 37 °C, 60 rpm for 14 days. As shown in Figure 4j, apparent burst release of exosomes occurs from the GM during the initial three days, and the release amounts are relatively low in the following days. However, GM@PDA exhibited a sustained release ($\approx 24.1\%$ in 3 days, $\approx 63.7\%$ in 7 days, $\approx 87.5\%$ in 10 days, and $\approx 94.5\%$ in 14 days) of increasing amounts of exosomes for a more extended period.

To verify whether GM@PDA&SHED-Exos micro-nano composites better rescue the impaired function of aged stem cells, AT-SCs were treated with GM, GM@PDA, and GM@PDA&SHED-Exos respectively in vitro. Compared with the GM and GM@PDA groups, the GM@PDA&SHED-Exos group showed a decrease in the number of β -gal-positive cells (Figure S5a, Supporting Information). Western blotting results showed that GM@PDA&SHED-Exos remarkably reduced the protein levels of senescence-related marker P21 (Figure S5b, Supporting Information). Moreover, pretreatment with GM@PDA&SHED-Exos promoted collagen matrix deposition and the expression of tenogenic markers FMOD and TNC, as shown by Sirius red staining, immunofluorescence staining, and western blotting (Figure S5c–e, Supporting Information). Interestingly, GM@PDA&SHED-Exos also inhibited the biased osteogenic differentiation of the AT-SCs, as evidenced by reduced calcium nodules and declined expression of osteogenesis-related genes *Alp* and *Bgalp* (Figure S5f,g, Supporting Information).

To demonstrate whether GM@PDA&SHED-Exos could firmly adhere to tendon tissues, we injected the GM@PDA&SHED-Exos and observed that these microspheres could be evenly distributed on the surfaces of tendon tissues (Figure S6a, Movie S1, Supporting Information). To investigate the biodistribution and retention of the GM@PDA&SHED-Exos in vivo, PKH26-labeled exosomes were synthesized and injected into rat tendons. Weak fluorescence signals of the PKH26-labeled free SHED-Exos were detected in tendons at 6 h, whereas GM@PDA&PKH26-SHED-Exos showed strong red fluorescence in tendons. Notably, the fluorescence signal of GM@PDA&PKH26-SHED-Exos existed for more than seven days and decreasing in a slow tendency, indicating that the GM@PDA was an effective delivery vehicle for SHED-Exos in local tendon tissues (Figure S6b,c, Supporting Information).

3.5. Local Administration of SHED-Exo-Loaded-Hydrogel Microspheres Efficiently Promotes Recovery of Tendinopathies and Partially Incised Tendons

Cell senescence contributes to the progression of collagenase-I-induced tendinopathy even in young populations.^[21] Therefore, to demonstrate the therapeutic effects of the local injection of GM@PDA&SHED-Exos on tendon injuries at the

young stage, we first established a three-month-old mouse Achilles tendinopathy model that was induced by collagenase I (Figure 5a). We injected GM@PDA&SHED-Exos thrice at zero, one, and two weeks with a 10 mg microsphere solution. Four weeks after injury, tendons from the GM@PDA&SHED-Exos groups displayed smoother contours, whereas tendons from the GM and GM@PDA groups still presented a red and swollen appearance (Figure 5b). Micro-CT images showed small ectopic bone formation in the GM@PDA&SHED-Exos groups (Figure 5c). Tendon is responsible for transferring the mechanical force from the muscle to the bone.^[22] To evaluate the locomotion performance of healing tendons, the AFI was recorded, where a more negative AFI value represented more serious hypomotility.^[23] After four weeks of injection, the GM@PDA&SHED-Exos-treated tendons showed a small negative AFI value close to that of the normal tendons, reflecting better motility and larger grip strength than the GM and GM@PDA groups (Figure 5d,e). HE staining showed that local injection of GM@PDA&SHED-Exos largely attenuated the formation of vacuole-like structures and promoted recovery of the aligned collagen structure, compared with the other groups (Figure 5f). SEM showed that the GM@PDA&SHED-Exos group possessed better collagen alignment after four weeks compared with the other groups, which revealed that GM@PDA&SHED-Exos better performed its therapeutic effect (Figure 5g). Moreover, GM@PDA&SHED-Exos alleviated cartilage matrix deposition, as evidenced by the lower expression of chondrogenic markers COL2 and AGGRECAN (Figure 5h). Immunofluorescence staining showed that there were larger clusters of CD146 positive cells that were accompanied by a reduced expression of senescence-related marker P21 in tendons from GM@PDA&SHED-Exos groups at four weeks postoperatively (Figure 5i). Overall, local intervention with GM@PDA&SHED-Exos could efficiently inhibit the progression of collagenase-I-induced tendinopathies in three-month-old young adult mice.

To further verify the better therapeutic effect of GM@PDA&SHED-Exos on tendon injuries at the relatively old stage, 18-month-old rats were partially incised as previously described^[10] and subsequently injected with all types of microspheres at zero, one, and two weeks after tendon injuries with a 20 mg microsphere solution (Figure 6a). After injection for eight weeks, all groups except the GM@PDA&SHED-Exos group displayed unusual swelling and shrinking (Figure 6b). Compared with the GM and GM@PDA groups, the GM@PDA & SHED-Exos-treated tendons had smaller negative AFI values close to those of the normal uninjured tendons, indicating better motility and larger grip strength at eight weeks (Figure 6c). Micro-CT images indicated smaller ectopic bone formation in the GM@PDA&SHED-Exos groups (Figure 6d). Local injection of GM@PDA&SHED-Exos largely attenuated the formation of vacuole-like structures and promoted the recovery of aligned collagen structures compared with local injection of the other groups (Figure 6e). Immunofluorescence staining showed that local injection of GM@PDA&SHED-Exos resulted in higher expression of tenogenic markers TNC and TNMD after eight weeks, which revealed that GM@PDA&SHED-Exos better performed its therapeutic effect (Figure 6f). Moreover, GM@PDA&SHED-Exos alleviated cartilage matrix deposition, as evidenced by the Alcian blue staining and lower expression of

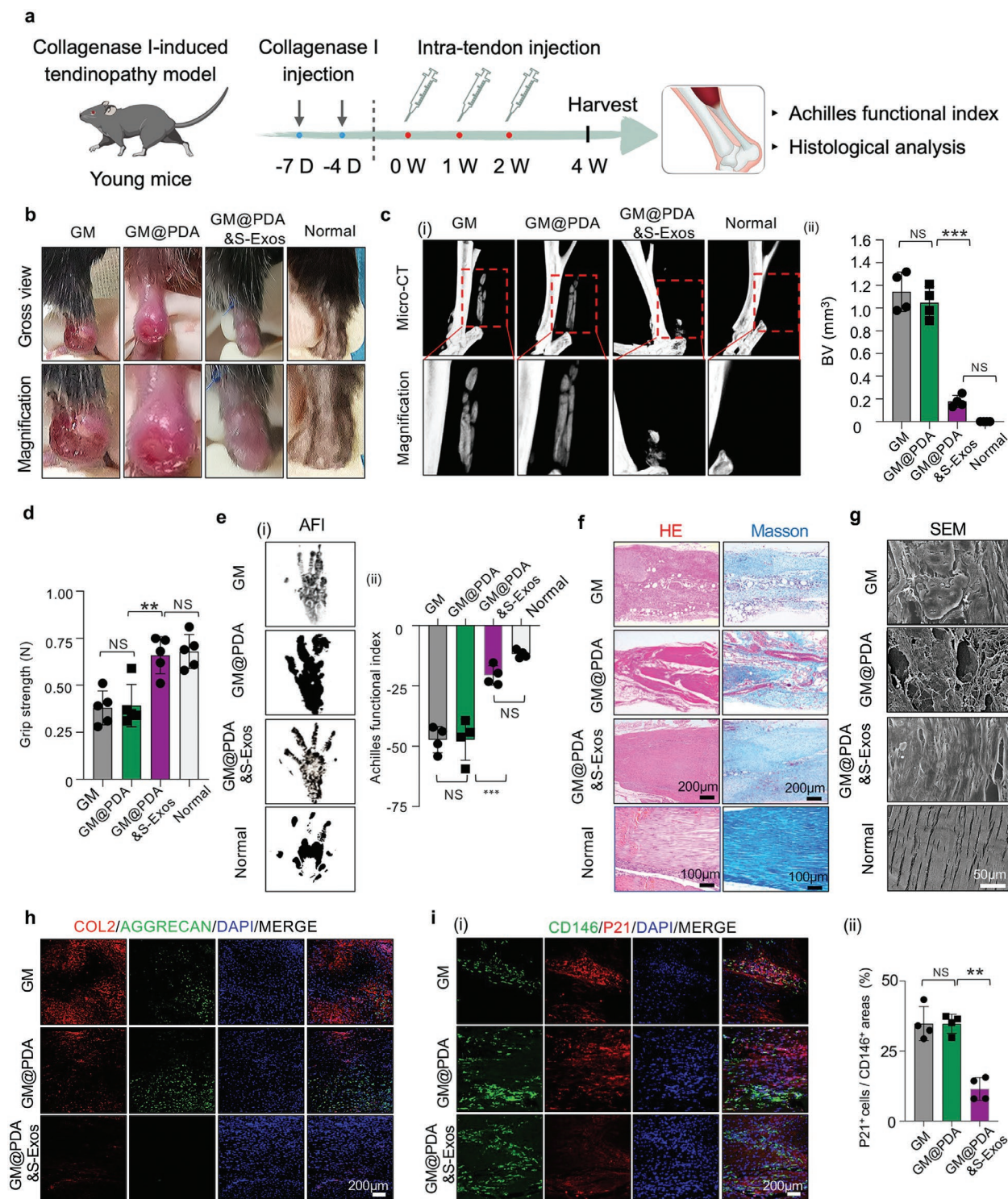


Figure 5. Local administration of hydrogel microspheres loaded with SHED-Exo nanoparticles efficiently delays the progression of collagenase I-induced tendinopathies in three-month-old young adult mice. a) Scheme of local delivery design. b) Gross view of skin contours of tendons in the fourth week postoperatively. c) Micro-CT scans of repaired Achilles tendons of each group in the fourth week postoperatively. ii) Semi-quantification of (i) ($n = 4$ mice per group). d) Grip strength of experimental mice from each group after four weeks ($n = 5$ mice per group). e) i) Footprints of experimental mice from different groups in the fourth week postoperatively. ii) Semi-quantification of AFI ($n = 4$ mice per group). f) HE and Masson's trichrome stainings of tendons from different groups in the fourth week postoperatively ($n = 4$ mice per group). g) SEM of tendons from different groups in the fourth week postoperatively ($n = 4$ mice per group). h) Immunofluorescence staining of COL2 and AGGRECAN of sections of each group in the fourth week postoperatively. i) i) Immunofluorescence staining of CD146 and P21 of sections of each group in the fourth week postoperatively. ii) Semi-quantification of (i) ($n = 4$ mice per group). Data are represented as mean \pm SD. Statistical significance was determined by one-way ANOVA with Tukey's test (NS: not significant; * $p < 0.05$; ** $p < 0.01$; *** $p < 0.001$).

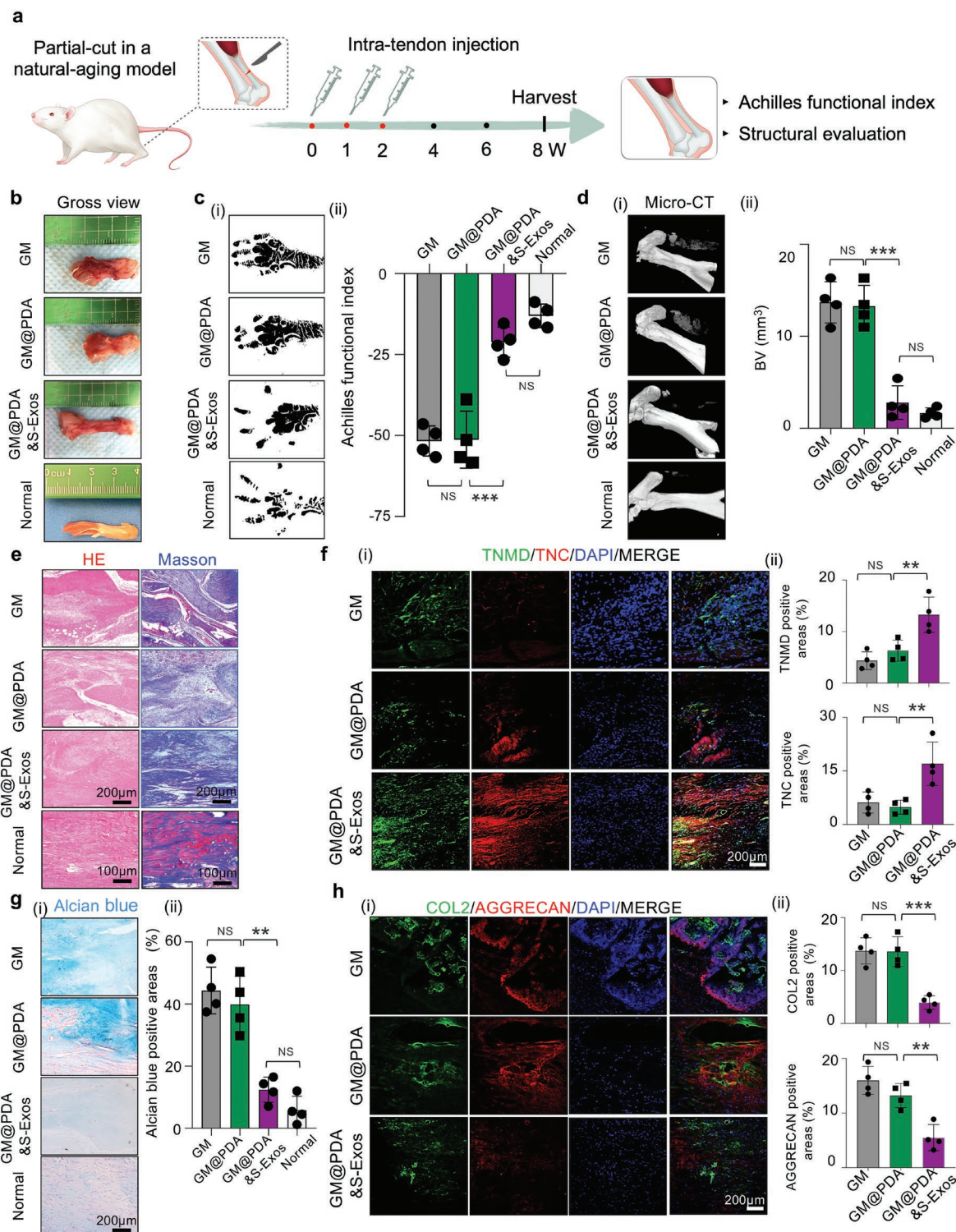


Figure 6. Local injection of SHED-Exos-loaded hydrogel microspheres rescues impaired endogenous reparative capacity in aged rats. a) Scheme of local delivery design. b) Overall view of repaired tendons in the eighth week postoperatively ($n = 4$ rats per group). c) i) Footprints of normal rats and experimental rats from different groups in the eighth week postoperatively. ii) Semi-quantification of AFI ($n = 4$ rats per group). d) i) Micro-CT scans of normal and repaired Achilles tendons of each group in the eighth week postoperatively ($n = 4$ rats per group). ii) Semi-quantification of (i) ($n = 4$ rats per group). e) HE and Masson's trichrome stainings of tendons from different groups in the eighth week postoperatively ($n = 4$ rats per group). f) i) Immunofluorescence staining of TNC and TNMD of sections of each group in the eighth week postoperatively. ii) Semi-quantification of (i) ($n = 4$ rats per group). g) Alcian blue stainings of tendons from different groups in the eighth week postoperatively ($n = 4$ rats per group). ii) Semi-quantification of (i) ($n = 4$ rats per group). h) i) Immunofluorescence staining of COL2 and AGGRECAN of sections of each group in the eighth week postoperatively. ii) Semi-quantification of (i) ($n = 4$ rats per group). Data are represented as mean \pm SD. Statistical significance was determined by one-way ANOVA with Tukey's test (NS: not significant; * $p < 0.05$; ** $p < 0.01$; *** $p < 0.001$).

chondrogenic markers COL2 and AGGRECAN (Figure 6g,h). In addition, SEM also showed that the neotendons in the GM@PDA&SHED-Exos group possessed the best collagen alignment after eight weeks (Figure S7, Supporting Information), although a small gap still existed compared to normal tendons. Progression of senescence retards tissue injury.^[24] Immunofluorescence staining showed that there was reduced expression of senescence-related index P21 or γ H2AX in the tendons from the GM@PDA&SHED-Exos group in the eighth week postoperatively (Figure S8a, Supporting Information). Moreover, after the local injection of GM@PDA&SHED-Exos, inflammatory infiltration in the tendons was reduced, which was accompanied by a decrease in the number of p65-positive cells. Similarly, intervention with GM@PDA&SHED-Exos also efficiently decreased the percentage of H3K27me3 positive cells (Figure S8b, Supporting Information). Consistent with the in vitro results, this finding further demonstrated that SHED-Exos reduced the accumulation of senescent cells by modulating histone methylation.

4. Discussion

As age increases, individuals with tendon injuries or defects frequently have impaired reparative and regenerative capacities owing to the hypofunction of TSPCs.^[25] To address this problem, we developed SHED-Exos-loaded hydrogel microspheres for local therapeutic interventions for tendinopathies and partially-incised tendons. The GM@PDA&SHED-Exos micro-nano composite exhibited a favorable pro-proliferation activity and an anti-senescent effect in vitro. More importantly, the micro-nano composite maintained the AT-SC tenogenic differentiation capacity and inhibited the biased osteogenic capacity of AT-SCs. As an in vivo therapeutic measure, GM@PDA&SHED-Exos were conveniently injected into injured tendons conveniently, whereby the controlled release of SHED-Exo nanoparticles effectively modulated the local AT-SC percentage and tenogenic potential to promote the repair and regeneration of damaged tendons. Previous investigations have shown that aggravated heterotopic ossification can hamper tendon regeneration.^[26] We observed that GM@PDA&SHED-Exos had additional therapeutic effects on reducing heterotopic ossification, possibly by inhibiting NF- κ B. Furthermore, persistent inflammation from senescent cells could retard the process of tendon repair.^[21] In the present study, local delivery of GM@PDA&SHED-Exos efficiently reduced the ratio of senescent cells and the secretion of inflammatory factors in the tendon in the eighth week postoperatively.

Senescent mesenchymal stem cells (MSCs) are crucial therapeutic targets for preventing tissue degeneration and can be rejuvenated by gene editing, small-molecule intervention, and microbiota modulation.^[27] Our previous research has revealed that the difference in the TSPC stemness between neonatal and adult stages influenced TSPC biological properties and adult tendon regeneration.^[10] Thus, a reasonable stemness-modulation method is a promising strategy for remedying AT-SCs and promoting the recovery of tendon injuries or tendinopathies. It has been reported that MSC-derived secretory factors or conditional media may effectively remedy neurodegenera-

tive diseases, neural injuries, cartilage, and bone defects via a paracrine mechanism.^[28] Moreover, MSCs-derived exosomes can interact with various cells and are safe for us as a potential therapeutic tool for different diseases.^[29] Compared with MSCs isolated from bone marrow, the paracrine products from SHEDs have a higher anti-apoptotic and pro-angiogenic composition and superior immunomodulatory effects in vitro.^[30] Recently, some studies have also revealed that SHEDs could play a therapeutic role in some aging-related diseases, such as irradiation-induced skin senescence and periodontal diseases.^[30,31] Our results revealed that SHED-Exos could rescue the impaired function of AT-SCs by coordinately inhibiting cellular senescence and maintaining the expression of critical stemness factors Sox2 and Oct4. Furthermore, SHED-Exo treatment in vivo ameliorated hallmarks of aging, including expression of the senescence markers and inflammatory infiltration. Future studies using large animals and humans are needed to promote the clinical application of the natural bioactive SHED-Exo nanoparticles in tendon diseases.

Epigenetic alterations are recognized as the hallmarks of cellular senescence or organism aging.^[32] Moreover, histone modification is considered as a crucial factor.^[33] Our results showed that SHED-Exos reduced the abundance of H3K9me3 and H3K27me3. After treatment with a pan-inhibitor of histone demethylases—JIB 04,^[34] the anti-senescence and pro-tenogenic effects of SHED-Exos were partially counteracted. H3K9me3 and H3K27me3 are two crucial histone modifications closely related to cell senescence and tissue aging.^[35] Previous in vitro experiments have revealed that a relatively low methylation level of H3K9me3 and H3K27me3 is a hinge for preserving the pluripotency of embryonic stem cells.^[36] Ye et al. have also reported that the accumulation of H3K9me3 and H3K27me3 positive cells remarkably intensified compared to the young controls in the bone marrow of aged mice.^[37] Here, our in vitro and in vivo results showed that levels of H3K9me3 and H3K27me3 were reduced after the SHED-Exos treatment, which could also indicate the stemness-modulation function of SHED-Exos. Exosomes-bearing proteins, lipids, RNAs, and DNAs have emerged as vital biological mediators in cell-to-cell communication.^[27,38] Our proteomics analysis showed that protein expressions of DPSC-Exos and SHED-Exos significantly differed, which may be responsible for the anti-aging function of SHED-Exos. These proteins could interact with histone methyltransferase and histone demethylase (SETD1B or KDM4B, KDM4D, KDM6B and LSD1) to modulate the levels of histone methylation and inhibit NF- κ B.^[34,39] However, we cannot dismiss that SHED-Exos also modify histone methylation through RNAs and lipids. In the future, it would be intriguing to explore whether SHED-Exos transfer functional proteins into AT-SCs to modulate the histone methylation, which may further amplify the anti-aging and pro-reparative effectiveness of SHED-Exos.

Overactivation of NF- κ B could be induced by long-term inflammatory insults or tissue injury. More importantly, dysregulation of NF- κ B could aggravate the progression of tendinopathies and impede tendon repair.^[40] Moreover, persistent activation of NF- κ B could bring about low-grade inflammation infiltration that would sink stem cells into senescence or aggravate cell hypofunction.^[41] Recently, many studies have indicated that NF- κ B serves as a crucial driving force of aging and a preferential

interventive target for inhibiting senescence.^[42] As extracellular vesicles from cells in the early embryonic phase, SHED-Exos could efficiently suppress the activation of NF- κ B due to TNF- α stimulation, which may explain the increased self-renewal and differentiation capacity, and decreased cell senescence in SHED-Exos-treated AT-SCs. Similar to existing anti-senescent therapies, an effective intervening measure that can orchestrate anti-senescent function simply is improbable, because it is widely accepted to be a complex process.^[41] This present study suggested that modulation of dual targets may represent a more efficient and promising strategy for tendon-associated diseases.

5. Conclusion

Based on the concept of harnessing the anti-senescent function of the natural bioactive nanoparticles, we observed that SHED-Exos could efficiently inhibit AT-SC senescent phenotypes and rescue their tenogenic differentiation capacity. Mechanistically, SHED-Exos primarily functioned through inhibiting histone methylation and suppressing the overactivation of NF- κ B. Finally, the local delivery of SHED-Exo bio-nanoparticles by hydrogel microspheres exhibited excellent anti-aging effects, including reducing senescent cells and decreasing ectopic bone formation, and thereby functionally and structurally rescued endogenous tendon regeneration and repair capacity in aged rats. The current findings open new avenues for the development of exosome-based therapies for age-related diseases.

Supporting Information

Supporting Information is available from the Wiley Online Library or from the author.

Acknowledgements

S.J. and Y.W. contributed equally to this work. This work was supported by National Natural Science Foundations of China 82230030 and 81871492 (Y.L.), 81930026 (Y.S.Z.), 82100980 (S.S.J.), 82201020 (Y.W.), 81901054 (Y.T.N.), Beijing International Science and Technology Cooperation Project Z221100002722003 (Y.L.), Ten-Thousand Talents Program QNBJ2019-2 (Y.L.), Key R & D Plan of Ningxia Hui Autonomous Region 2020BCG01001 (Y.L.), Innovative Research Team of High-level Local Universities in Shanghai (SHSMU-ZLXC20212402, Y.L.), Beijing Nova Program Z211100002121043 (Y.W.), Beijing Natural Science Foundation 7214305 (S.S.J.), the China National Postdoctoral Program for Innovative Talents BX2021022 (Y.W.) and BX20200020 (S.S.J.), China Postdoctoral Science Foundation 2021M700281 (Y.W.) and 2019M660010 (Y.T.N.), and National Key Clinical Specialty Construction Project (PKUSSNMP-201902).

Conflict of Interest

The authors declare no conflict of interest.

Data Availability Statement

The data that support the findings of this study are available from the corresponding author upon reasonable request.

Keywords

exosome nanoparticles, hydrogel microspheres, senescence, tendon regeneration, tendon stem/progenitor cells

Received: December 12, 2022

Revised: January 19, 2023

Published online:

- [1] G. C. Dai, Y. J. Li, M. H. Chen, P. P. Lu, Y. F. Rui, *World J. Stem Cells* **2019**, *11*, 677.
- [2] H. L. Birch, M. J. Peffers, P. D. Clegg, *Adv. Exp. Med. Biol.* **2016**, *920*, 247.
- [3] D. K. Jeppesen, A. M. Fenix, J. L. Franklin, J. N. Higginbotham, Q. Zhang, L. J. Zimmerman, D. C. Liebler, J. Ping, Q. Liu, R. Evans, W. H. Fissell, J. G. Patton, L. H. Rome, D. T. Burnette, R. J. Coffey, *Cell* **2019**, *177*, 428.
- [4] a) M. Mathieu, L. Martin-Jaular, G. Lavieu, C. Théry, *Nat. Cell Biol.* **2019**, *21*, 9; b) T. Liu, Q. Zhang, J. Zhang, C. Li, Y. R. Miao, Q. Lei, Q. Li, A. Y. Guo, *Nucleic Acids Res.* **2019**, *47*, D89; c) H. M. Zhang, Q. Li, X. Zhu, W. Liu, H. Hu, T. Liu, F. Cheng, Y. You, Z. Zhong, P. Zou, Q. Li, Z. Chen, A. Y. Guo, *Cancer Res.* **2016**, *76*, 2901.
- [5] a) C. P. Lai, X. O. Breakefield, *Front. Physiol.* **2012**, *3*, 228; b) Y. Wang, X. Lu, J. He, W. Zhao, *Stem Cell Res. Ther.* **2015**, *6*, 100; c) F. Prattichizzo, A. Giuliani, J. Sabbatinelli, E. Mensà, V. De Nigris, L. La Sala, P. de Candia, F. Olivieri, A. Ceriello, *J. Extracell. Vesicles* **2019**, *8*, 1656044.
- [6] a) T. Yamaza, A. Kentaro, C. Chen, Y. Liu, Y. Shi, S. Gronthos, S. Wang, S. Shi, *Stem Cell Res. Ther.* **2010**, *1*, 5; b) T. Yamaza, F. S. Alatas, R. Yuniartha, H. Yamaza, J. K. Fujiyoshi, Y. Yanagi, K. Yoshimaru, M. Hayashida, T. Matsuura, R. Aijima, K. Ihara, S. Ohga, S. Shi, K. Nonaka, T. Taguchi, *Stem Cell Res. Ther.* **2015**, *6*, 171.
- [7] a) J. K. Bar, A. Lis-Nawara, P. G. Grelewski, *Int. J. Mol. Sci.* **2021**, *22*, 12018; b) V. D. Zingale, A. Gugliandolo, E. Mazzon, *Int. J. Mol. Sci.* **2021**, *23*, 90; c) H. Oubenyahya, *Chin. J. Dent. Res.* **2021**, *24*, 9; d) P. Liu, Q. Zhang, J. Mi, S. Wang, Q. Xu, D. Zhuang, W. Chen, C. Liu, L. Zhang, J. Guo, X. Wu, *Stem Cell Res. Ther.* **2022**, *13*, 89.
- [8] Y. Xie, L. Yu, Z. Cheng, Y. Peng, Z. Cao, B. Chen, Y. Duan, Y. Wang, *J. Nanobiotechnol.* **2022**, *20*, 239.
- [9] Z. Yuan, X. Yuan, Y. Zhao, Q. Cai, Y. Wang, R. Luo, S. Yu, Y. Wang, J. Han, L. Ge, J. Huang, C. Xiong, *Small* **2021**, *17*, e2006596.
- [10] Y. Wang, S. Jin, D. Luo, D. He, C. Shi, L. Zhu, B. Guan, Z. Li, T. Zhang, Y. Zhou, C. Y. Wang, Y. Liu, *Nat. Commun.* **2021**, *12*, 1293.
- [11] R. Ren, A. Ocampo, G. H. Liu, J. C. Izpisua Belmonte, *Cell Metab.* **2017**, *26*, 460.
- [12] R. Liu, B. Zhou, H. Zhang, Y. Chen, C. Fan, T. Zhang, T. Qin, J. Han, S. Zhang, X. Chen, W. Shen, J. Chang, Z. Yin, *Chem. Eng. J.* **2021**, *420*, 129415.
- [13] P. P. Y. Lui, X. Zhang, S. Yao, H. Sun, C. Huang, *Int. J. Mol. Sci.* **2022**, *23*, 3571.
- [14] J. Crouch, M. Shvedova, R. Thanapaul, V. Botchkarev, D. Roh, *Cells* **2022**, *11*, 672.
- [15] D. H. Zineldeen, H. Uranishi, T. Okamoto, *Curr. Drug Metab.* **2010**, *11*, 266.
- [16] K. Xu, C. Lin, D. Ma, M. Chen, X. Zhou, Y. He, S. A. A. Moqbel, C. Ma, L. Wu, *Oxid. Med. Cell Longevity* **2021**, *2021*, 5519587.
- [17] J. Chang, Z. Wang, E. Tang, Z. Fan, L. McCauley, R. Franceschi, K. Guan, P. H. Krebsbach, C. Y. Wang, *Nat. Med.* **2009**, *15*, 682.
- [18] J. Duan, X. Liang, J. Guo, K. Zhu, L. Zhang, *Adv. Mater.* **2016**, *28*, 8037.
- [19] Y. Lei, Y. Wang, J. Shen, Z. Cai, Y. Zeng, P. Zhao, J. Liao, C. Lian, N. Hu, X. Luo, W. Cui, W. Huang, *Adv. Funct. Mater.* **2021**, *31*, 2105084.

- [20] a) J. Shen, A. Chen, Z. Cai, Z. Chen, R. Cao, Z. Liu, Y. Li, J. Hao, *Bioact. Mater.* **2022**, *12*, 153; b) H. Lee, S. M. Dellatore, W. M. Miller, P. B. Messersmith, *Science* **2007**, *318*, 426; c) H. A. Lee, E. Park, H. Lee, *Adv. Mater.* **2020**, *32*, 1907505.
- [21] S. Y. Chen, I. M. Jou, P. Y. Ko, K. L. Hsu, W. R. Su, L. C. Kuo, P. Y. Lee, C. L. Wu, P. T. Wu, *Mol. Ther.–Methods Clin. Dev.* **2022**, *26*, 157.
- [22] D. Docheva, S. A. Müller, M. Majewski, C. H. Evans, *Adv. Drug Delivery Rev.* **2015**, *84*, 222.
- [23] S. Yang, X. Shi, X. Li, J. Wang, Y. Wang, Y. Luo, *Biomaterials* **2019**, *207*, 61.
- [24] a) V. Moiseeva, A. Cisneros, A. C. Cobos, A. B. Tarrega, C. S. Oñate, E. Perdiguero, A. L. Serrano, P. Muñoz-Cánoves, *FEBS J.* **2022**; b) T. G. Bird, M. Müller, L. Boulter, D. F. Vincent, R. A. Ridgway, E. Lopez-Guadamillas, W. Y. Lu, T. Jamieson, O. Govaere, A. D. Campbell, S. Ferreira-Gonzalez, A. M. Cole, T. Hay, K. J. Simpson, W. Clark, A. Hedley, M. Clarke, P. Gentaz, C. Nixon, S. Bryce, C. Kiourtis, J. Sprangers, R. J. B. Nibbs, N. Van Rooijen, L. Bartholin, S. R. McGreal, U. Apte, S. T. Barry, J. P. Iredale, A. R. Clarke, et al., *Sci. Transl. Med.* **2018**, *10*, eaan1230.
- [25] P. P. Y. Lui, C. M. Wong, *Front. Genet.* **2019**, *10*, 1338.
- [26] M. D. Caceres, K. Angerpointner, M. Galler, D. Lin, P. A. Michel, C. Brochhausen, X. Lu, A. R. Varadarajan, J. Warfsmann, R. Stange, V. Alt, C. G. Pfeifer, D. Docheva, *Cell Death Dis.* **2021**, *12*, 1049.
- [27] Q. Lei, F. Gao, T. Liu, W. Ren, L. Chen, Y. Cao, W. Chen, S. Guo, Q. Zhang, W. Chen, H. Wang, Z. Chen, Q. Li, Y. Hu, A. Y. Guo, *Sci. Transl. Med.* **2021**, *13*, eaaz8697.
- [28] S. Fernández-Francos, N. Eiro, L. A. Costa, S. Escudero-Cernuda, M. L. Fernández-Sánchez, F. J. Vizoso, *Int. J. Mol. Sci.* **2021**, *22*, 8395.
- [29] M. Kou, L. Huang, J. Yang, Z. Chiang, S. Chen, J. Liu, L. Guo, X. Zhang, X. Zhou, X. Xu, X. Yan, Y. Wang, J. Zhang, A. Xu, H. F. Tse, Q. Lian, *Cell Death Dis.* **2022**, *13*, 580.
- [30] M. Ueda, Y. Nishino, *J. Craniofacial Surg.* **2010**, *21*, 1861.
- [31] T. Saskianti, A. P. Nugraha, C. Prah santi, D. S. Ernawati, K. Tanimoto, W. Riawan, M. Kanawa, T. Kawamoto, K. Fujimoto, *Clin., Cosmet. Invest. Dent.* **2022**, *14*, 71.
- [32] C. Huidobro, A. F. Fernandez, M. F. Fraga, *Mol. Aspects Med.* **2013**, *34*, 765.
- [33] Y. Wang, Q. Yuan, L. Xie, *Curr. Stem Cell Res. Ther.* **2018**, *13*, 125.
- [34] L. Wang, J. Chang, D. Varghese, M. Dellinger, S. Kumar, A. M. Best, J. Ruiz, R. Bruick, S. Peña-Llopis, J. Xu, D. J. Babinski, D. E. Frantz, R. A. Brekken, A. M. Quinn, A. Simeonov, J. Easmon, E. D. Martinez, *Nat. Commun.* **2013**, *4*, 2035.
- [35] P. D'Aquila, G. Rose, D. Bellizzi, G. Passarino, *Maturitas* **2013**, *74*, 130.
- [36] B. W. Carey, L. W. Finley, J. R. Cross, C. D. Allis, C. B. Thompson, *Nature* **2015**, *518*, 413.
- [37] L. Ye, Z. Fan, B. Yu, J. Chang, K. Al Hezaimi, X. Zhou, N. H. Park, C. Y. Wang, *Cell Stem Cell* **2012**, *11*, 50.
- [38] M. Yoshida, A. Satoh, J. B. Lin, K. F. Mills, Y. Sasaki, N. Rensing, M. Wong, R. S. Apte, S. I. Imai, *Cell Metab.* **2019**, *30*, 329.
- [39] a) E. L. Greer, Y. Shi, *Nat. Rev. Genet.* **2012**, *13*, 343; b) A. Maiques-Diaz, L. Nicosia, N. J. Basma, I. Romero-Camarero, F. Camera, G. J. Spencer, F. M. R. Amaral, F. Simeoni, B. Wingelhofer, A. J. K. Williamson, A. Pierce, A. D. Whetton, T. C. P. Somerville, *Oncogene* **2022**, *41*, 4841; c) Y. Zhan, W. Qiao, B. Yi, X. Yang, M. Li, L. Sun, L. Ji, P. Su, X. Wang, F. Zhang, R. Zhang, M. Gao, W. Zhao, Y. Song, *Oncogene* **2022**, *41*, 4512.
- [40] A. C. Abraham, S. A. Shah, M. Golman, L. Song, X. Li, I. Kurtalaj, M. Akbar, N. L. Millar, Y. Abu-Amer, L. M. Galatz, S. Thomopoulos, *Sci. Transl. Med.* **2019**, *11*, eaav4319.
- [41] S. An, S. Y. Cho, J. Kang, S. Lee, H. S. Kim, D. J. Min, E. Son, K. H. Cho, *Proc. Natl. Acad. Sci. USA* **2020**, *117*, 31535.
- [42] a) F. G. Osorio, C. Soria-Valles, O. Santiago-Fernández, J. M. Freije, C. López-Otín, *Int. Rev. Cell Mol. Biol.* **2016**, *326*, 133; b) A. Salminen, A. Kauppinen, K. Kaarniranta, *Cell Signal* **2012**, *24*, 835; c) Y. Wang, L. Wang, X. Wen, D. Hao, N. Zhang, G. He, X. Jiang, *Mech. Ageing Dev.* **2019**, *184*, 111160.